Perturbation dynamics of a planktonic ecosystem

Katherine Healey[1]
katiehealey@shaw.ca

Adam H. Monahan[1]
monahana@uvic.ca

Debby Ianson[2]
debby.ianson@pac.dfo-mpo.gc.ca

[1] School of Earth and Ocean Sciences, University of Victoria, PO Box 3055 STN CSC, Victoria, British Columbia, V8W 3P6, Canada

[2] Fisheries and Oceans Canada, Institute of Ocean Sciences, PO Box 6000, Sidney, British Columbia, V8L 4B2, Canada

Submitted to Journal of Marine Research as an article August 20, 2008

Abstract

Planktonic ecosystems provide a key mechanism for the transfer of CO_2 from the atmosphere to the deep ocean via the so-called "biological pump". Mathematical models of these ecosystems have been used to predict CO_2 uptake in surface waters, and more recently have been embedded in global climate models. While the equilibrium properties of these models are well studied, less attention has been paid to their response to external perturbations, despite the fact that, as a result of the variability of environmental forcing, such ecosystems are rarely, if ever, in equilibrium. Human induced perturbations to these ecosystems, namely the addition of limiting nutrients (e.g. iron) to areas where nitrate is plentiful to accelerate the biological pump, have been proposed as a solution to reduce atmospheric CO_2. In this study, linear theory is used to determine the structure of initially "unit-norm" perturbations to state variables of a five state variable ecosystem model in steady state, describing Ocean Station P (50°N 145°W) in summer, that optimize either instantaneous export flux of organic matter at fixed times or integrated export as the ecosystem relaxes towards equilibrium. A common feature in the optimization experiments for both instantaneous and integrated flux is the synchronization of the oscillatory behavior between two state variables. Because of these oscillations, there is an indirect contribution to the export flux that is non-intuitive. For all perturbations, it is found that the flux to higher trophic levels is the primary contributor to export flux, and, contrary to expectations, the contribution of aggregation is negligible.

1. Introduction

Atmospheric carbon dioxide (CO_2) dissolves in the surface waters of the oceans, and phytoplankton fix some of this CO_2 through photosynthesis, transforming it into particulate organic carbon (POC). A portion of this POC, denoted exported carbon, eventually reaches the deep ocean, where it remains essentially out of contact with the atmosphere on climate time scales (i.e. 1000 years). This process is known as the "biological pump", and enhances the ocean's ability to store carbon (Sarmiento and Gruber, 2006, Volk and Hoffert, 1985). Although phytoplankton growth is often limited by light or nutrients, it is not, in general, limited by carbon, and an increase in atmospheric CO_2 will not directly accelerate the biological pump.

There are large areas of the ocean where major nutrients (e.g. nitrogen), the lack of which is limiting to photosynthesis, are available and not drawn down to limiting concentrations by primary production. These are called high nutrient low chlorophyll (HNLC) regions, and include the subarctic North Pacific and Southern Ocean (de Baar *et al.*, 2005). Martin *et al.* (1989, 1991) hypothesized that phytoplankton growth in HNLC regions is limited by the micronutrient iron, and it has been suggested that atmospheric CO_2 may be reduced by fertilizing HNLC areas with iron to enhance the biological pump. An increase in phytoplankton biomass has been observed following both natural (e.g. Jo *et al.*, 2007) and synthetic (e.g. Saito *et al.*, 2006) iron fertilization events, however exported carbon in response to these events may only be measured indirectly (e.g. Wong *et al.*, 2006). In general, blooms such as these have not been occupied long enough to observe responses in export; thus the effect of iron fertilization on export dynamics remains uncertain.

Because of the importance of export dynamics and possible changes to these dynamics under climate change, it is necessary to develop mechanistic and predictive models of planktonic ecosystems. Such models typically consist of a system of differential equations describing the temporal evolution of ecosystem variables (e.g. nutrients, phytoplankton, zooplankton (Fasham, 1993)). Real planktonic systems involve a large number of species displaying a bewildering complexity of physiological states, nutrient requirements, and trophic interactions. In planktonic ecosystem models, one is not able to model this complexity: rather, phytoplankton and zooplankton are divided into what are termed 'functional groups', defined by common ecosystem-scale characteristics.

Many formulations for modeling ecosystem dynamics have been proposed, and ecosystem models varying in complexity from 3 state variables (nutrient, phytoplankton (P), zooplankon (Z)) in a homogenous medium (e.g. Steele, 1974) to 3-dimensional models containing multiple functional groups of plankton and nutrients (e.g. Moore *et al.*, 2004) have been studied. In addition, many comprehensive global climate models that are used to study climate change have an ocean biology component that includes a simple planktonic ecosystem model (e.g. Schmittner *et al.*, 2005, Zahariev *et al.*, 2008). However, the dynamics of these ecosystem models are often poorly understood, particularly their response to a variable physical environment.

While the nonlinearity of these model equations generally limits the analytical study of model dynamics, useful insight can often be obtained through the study of local linearized dynamics around model equilibria (Perko, 2001). Continual physical forcing from the atmosphere and ocean mean that these ecosystems are never

in steady state (Monahan and Denman, 2004, hereafter referred to as MD04). If variability is not too large, the state of the ecosystem may be considered as a steady background state that is modified by some perturbation evolving according to locally linear dynamics. Such a linearization allows for a systematic analysis of the model dynamics for a small perturbation from steady state, and may provide qualitative information about the behaviour of perturbations that may not be considered "small". Locally linearized dynamics have been used to study the stability properties of model equilibria (e.g. Edwards and Brindley, 1999), but although it has been demonstrated that modelled phytoplankton populations can display rapid transient growth (e.g. Pitchford and Brindley, 1999, Truscott and Brindley, 1994), less attention has been paid to the dynamics of perturbations around steady states. The relationship between the evolution of ecosystems and export flux is complicated, and possibly counter-intuitive. Well established mathematical theory (e.g. Tziperman and Ioannou, 2002) may be used to determine perturbations to a steady state that lead to responses from the ecosystem that are "optimal" in some specified way, such as maximizing the export flux (rate of POC leaving the model domain). These perturbations represent small changes to an ecosystem state that may occur in response to external forcing by natural occurrences such as addition of iron by dust deposition, advection and mixing with an eddy that has a different concentration of state variables, or mixed layer depth variability in response to fluctuating atmospheric forcing.

This study considers the dynamics of a medium complexity (5 compartment) model, representative of the type of model currently being embedded in global climate

models. It was designed to simulate ecosystem processes at Ocean Station P (50°N 145°W), a HNLC region located in the subarctic northeast Pacific, where spring and summertime photosynthetic growth is thought to be limited by micronutrients such as iron. In this region, small phytoplankton are dominant and tightly coupled with microzooplankton, and diatom blooms are observed only occasionally (Boyd and Harrison, 1999). A wealth of historical data exist, and Station P was the site of the Subarctic Ecosystem Response to Iron Enrichment Study (SERIES), a synthetic iron fertilization experiment (Boyd *et al.*, 2004). The data show that chlorophyll remains approximately constant throughout the year despite considerable variability within the ecosystem (Wong *et al.*, 1999). Most of the time, the ecosystem at Station P appears to be near, or fluctuating about, steady state, and thus this setting is ideal for the analysis of small perturbations to equilibrium.

While this model is a highly idealized representation of the natural ecosystem, it is representative of the type of model currently being embedded in global climate models, so its dynamics are of interest for their implications regarding the ecosystem and these complex global models. The model is presented in Section 2, ecosystem and export responses to perturbations are presented in Section 3, and results are discussed in Section 4. Model details and linear optimization theory are discussed in Appendixes A and B, respectively.

2. Model

The planktonic ecosystem model used in this study is based on MD04 (Figure 1), but set in a 0-dimensional physical framework, i.e., a uniform mixed layer of fixed

depth. The ecosystem model is similar to those used in global models of the carbon cycle (e.g. Zahariev *et al.*, 2008). There are 2 functional groups of phytoplankton; small ($\leq 20\mu m$) phytoplankton, including flagellates (P_1), and large ($> 20\mu m$) phytoplankton, mainly diatoms (P_2). The phytoplankton are split into functional groups because small and large phytoplankton are grazed at different trophic levels, and P_2 are normally thought to be the most important contributor to export flux. Microzooplankton (Z_1) are modeled explicitly, and are tightly coupled with their prey, which are small phytoplankton and dead organic matter, termed detritus (D). Mesozooplankton (Z_2) graze on larger prey items, which in this model are P_2 and Z_1; time scales for changes in Z_2 biomass are much longer than for phytoplankton and microzooplankton, and thus Z_2 is specified at the maximum value of the observed annual cycle (Goldblatt *et al.*, 1999) in order to simulate summer conditions. The only nutrient explicitly modeled, and so the only potentially limiting nutrient in the model, is nitrogen (N). A full mathematical description of the ecosystem model is given in Appendix A. Table 1 contains definitions of symbols that are frequently used in this study, including state variables.

Of the four steady states found for this model (Healey, 2008), only one steady state is stable (Table 2), that is, small perturbations to this equilibrium will result in a return to this state. It also corresponds to a reasonable representation of conditions at Station P. While this steady state is asymptotically stable, some perturbations may display growth over finite times. The perturbation dynamics around this equilibrium will be the focus of this study. Perturbations (of initial magnitude $1 mmol N m^{-3}$) that optimize export flux from the ecosystem are solved for (see

Appendix B for methods), and responses to perturbations that display the highest export flux, relative to the initial export flux, are presented and discussed in Section 3. Note that because we consider the linearized model dynamics, the evolution of the perturbations is insensitve to the initial perturbation magnitude.

There are 3 pathways for the export of particulate matter from the ecosystem: sinking D (with no aggregation), flux to higher trophic levels as P_2 and Z_1 are grazed upon by Z_2, and aggregation of P_2 and D (Figure 1 bold arrows, (10). The third export pathway simulates the formation of marine snow in which larger phytoplankton and detritus form aggregates, which then sink (Alldredge and Silver, 1988) . Also note the implicit assumption that the matter going to higher trophic levels does not re-enter the surface layer of the ocean once it leaves.

Note that the analyses in this study consider only export of particulate organic carbon and neglect contributions of dissolved organic carbon to export flux. This assumption is reasonable as a first approximation; sediment trap data suggests that POC is the greatest contributor to export flux at 20m at Station P (Wong *et al.*, 1999).

The sinking D export flux depends linearly on D; however, the flux to higher trophic levels and aggregation terms are nonlinear and so must be linearized about the steady state in order to perform the optimizations (Appendix B). The linearized export in this case is given by

$$Export = 0.22P_2 + 0.21Z_1 + 0.38D \tag{1}$$

3. Results: Ecosystem and Export Flux Responses to Perturbations

a. Export flux

As discussed in Appendix B, we determine unit perturbations (initially unit norm changes in state variables) to a model steady state that optimize the instantaneous export fluxes at specified times τ. These "optimal perturbations" are calculated 10 times per day for fixed times between 0 and 30 days, so that there is sufficient resolution to observe the dependence of optimal perturbations on optimization time. Of the perturbations that optimize instantaneous export flux, the perturbation that results in the largest amplification (maximum instantaneous export flux relative to the initial export flux; given by (21)) is the perturbation that optimizes the export flux for $\tau = 9.3$ days, with a maximum amplification factor of 12.5 (Figure 2). The set of changes to the state variables in this case is referred to as Φ_{FLUX}, and its components are given in Table 3.

i. Ecosystem Response. The linearized response to Φ_{FLUX} is shown in Figure 4a. This initial perturbation consists primarily of an increase in P_2 (Table 3), that monotonically decreases, taking 75 days to drop to 10% of its initial value, and a decrease in Z_1 that allows a rapid bloom of P_1 which peaks at day 6.

The Z_1 recover due to the abundance of available food, reaching maximum biomass at day 11. The P_1 are then grazed below steady state value to a minimum at day 17, which leads to a local minimum of Z_1 occurring at day 22. Damped predator-prey oscillations (Volterra, 1928) continue to occur with a period of 22-23 days, with the P_1 leading the Z_1 by 5-6 days. Because the model has more than two

dimensions, predator-prey oscillations are not required to be about steady state; for most of the evolution of the perturbation, the P_1 remain above steady state value as the ecosystem approaches equilibrium, while Z_1 biomass oscillates about the steady state. The initial perturbation in P_1 is negligible, so that P_1 and Z_1 are synchronized relative to their predator-prey oscillation cycle with a lag of 5 days, allowing the maximum response in P_1.

Detritus biomass, and thus export flux of sinking D, reaches a maximum at 9 days, after the initial P_1 bloom peaks but before the Z_1 attain their maximum. This maximum of D occurs before the peak Z_1 for 2 reasons: a portion of the increased P_1 being grazed down by Z_1 enters the D pool via 'sloppy feeding', and there is less grazing of Z_1 on D at this time (4).

There is considerable drawdown in N (2-3 μM) with the concentration decreasing to a minimum of less than $6\mu M$ at 68.5 days (not shown). This decay in N results from the balance between P_2 uptake, with a long decay time, and the slow, steady supply of N from below. After this time, N concentrations begin to increase, albeit slowly, taking over a year to approach the former steady state value. In fact, the model dynamics governing incoming N are unrealistic: all N recovery is through upwelling and diffusion, as the model does not include horizontal mixing of nutrients. Furthermore, the model is set in a perpetual summer, with no winter deepening of the mixed layer. However, because the ecosystem is not N limited at any time, the N dynamics have no effect on the other state variables or export dynamics, which is the primary focus of this analysis.

ii. Export Response. All components of export flux increase initially in response to Φ_{FLUX} (Figure 5a). Export flux due to aggregation reaches a maximum at day 6, after the maximum in P_2 and before the maximum in D, and then decreases toward steady state. Export to higher trophic levels reaches a maximum at day 10, and net export increases to a maximum shortly before day 10, reflecting a compromise between export due to sinking D and flux to higher trophic levels. These maxima follow the maximum in P_1; increased grazing on P_1 produces D, which sinks and contributes to aggregation, and the increased Z_1 biomass increases the flux to higher trophic levels. The maximum aggregation occurs earliest, before P_2 mortality increases due to increased grazing of Z_2 on Z_1. There is a second peak in export flux around day 30, and export fluxes display damped oscillations on the time scale of predator-prey interactions, in response to these oscillations in P_1 and Z_1.

Both major export events follow blooms in P_1. The maximum instantaneous export flux is $4.4 mmol N m^{-2} d^{-1}$ (Table 4), the highest instantaneous export flux in response to any of the perturbations. Note that by construction, Φ_{FLUX} is the perturbation that gives the highest export flux relative to the initial export flux of the perturbation, with an amplification factor of 12.5 (Figure 6). The additional integrated export above steady state in response to this perturbation is $76 mmol N m^{-2}$ ($6.1 g C m^{-2}$ assuming a C:N ratio of 106:16, see Appendix A) over 150 days. Aside from the initial decreased flux of sinking detritus, all export rates remain above steady state export rates, primarily because P_1 and P_2 remain above their mean values.

b. Export flux, perturbation in P_1 and P_2

In the previous subsection, the optimal perturbations were permitted to involve all components of the ecosystem, and all model state variables were involved in mediating the responses to this perturbation. In particular, interactions between P_1 and Z_1 were seen to be an important aspect of the response. It is natural to ask how large a response can be generated from a perturbation in only the phytoplankton, such as a bloom. Thus, for this optimization (Appendix B), only perturbations in P_1 and P_2 were allowed, while Z_1, D, and N were held constant.

In this situation the amplification of the instantaneous export was much smaller than for Φ_{FLUX}. The perturbation that optimizes export flux at $\tau = 4.3$ days results in the maximum amplification of export flux by a factor of only 1.5. Although this amplification factor is small compared to the amplification of Φ_{FLUX}, instantaneous export still increases by more than 50% above the initial perturbation.

i. Ecosystem Response. The ecosystem response to Φ_{FLUX-P} is shown in Figure 4b. This perturbation is an increase in both P_1 and P_2 (Table 3). The P_2 decay time scale is slightly shorter than in response to Φ_{FLUX}; perturbed P_2 take 73 days to decay to 10% of the initial perturbation. The response to this perturbation is very similar to the response to Φ_{FLUX} but shifted by about 6 days; like Φ_{FLUX}, damped predator-prey oscillations follow the perturbation, with P_1 remaining above steady state and Z_1 fluctuating about steady state. The microzooplankton abundance Z_1 increases in response to the increase in P_1, reaching a maximum at 5 days. Detritus increases to a maximum at 4.3 days due to both sloppy feeding by Z_1 as the P_1 are

grazed down and to mortality of P_2. The N concentration decreases to a minimum around 70.5 days, and then gradually begins to recover.

ii. Export Response. All components of export flux increase immediately following Φ_{FLUX-P} (Figure 5b). The net export flux reaches a maximum at 4 days. While the export flux is dominated by flux to higher trophic levels, the magnitude of this flux decreases following the perturbation; sinking detritus increases significantly following the initial perturbation, and is the main contributor to the amplification of export. The initial perturbation does not change the amount of D present in the ecosystem, but increased D due to Z_1 grazing on P_1, and P_2 mortality, result in additional export of sinking D, to a maximum at 4 days. Although the maximum amplification factor in the case of Φ_{FLUX-P} is much smaller than in Φ_{FLUX}, the additional integrated export response to Φ_{FLUX-P} of $75 mmol N m^{-2}$ ($5.7 g C m^{-2}$) is only slightly less (Table 4).

c. Integrated flux

In the previous sections, instantaneous export flux was optimized at fixed times. These optimal perturbations may have little influence on the total amount of POC exported, as there is no guarantee that the transient export fluxes remain high as the ecosystem returns to equilibrium. The unit perturbation that maximizes the integrated export, i.e., the total amount of POC exported from the ecosystem as it returns to equilibrium, Φ_{INT}, is determined as presented in Appendix B.

i. Ecosystem Response. The linearized ecosystem response to the perturbation Φ_{INT} is shown in Figure 4c. This perturbation is primarily an increase in P_2 (Table 3). The other components of the initial perturbation conditions have a negligible effect on the ecosystem and export response; the responses to Φ_{INT} are nearly indistinguishable from the responses to a perturbation that only increases P_2, Φ_{P_2} (Table 4). This initial increase in P_2 decays slowly, taking more than 75 days to drop below 10% of its initial value.

As the perturbation evolves, the initial slight decrease in Z_1 is amplified and the Z_1 biomass reduced significantly below equilibrium value to a minimum at 4.5 days. The increase in P_2 increases the overall grazing rate of Z_2, causing this decrease in Z_1. This response differs from the Z_1 increase observed following Φ_{FLUX} because Φ_{INT} has almost no P_1 component, so there is no initial increase in flux to Z_1 biomass to offset the increased Z_2 grazing. The decrease in Z_1 results in less predation on P_1, D, and P_2 (indirectly), and allows an increase in P_1 that peaks at 9.6 days. This bloom increases the food availability of the Z_1, which respond by recovering to above-steady state values, peaking at 15.8 days. Like the response to Φ_{FLUX}, damped predator-prey oscillations continue in P_1 and Z_1. At no time does the P_1 biomass drop below steady state, while the Z_1 biomass oscillates about its equilibrium value. Detritus values reach a maximum at 12.0 days.

ii. Export Response. The perturbation Φ_{INT} is primarily an increase in P_2, which results in an immediate increased flux to higher trophic levels, and thus net export (Figure 5c). The increased flux to higher trophic levels (Z_2 grazing) results in a decrease of Z_1, and a local minimum of both flux to higher trophic levels and net

export. Damped oscillations driven by the predator-prey cycle between Z_1 and P_1 follow. Following the maxima caused by the initial P_1 bloom, all export components decrease. At no time do any of the export rates drop below steady state values.

The perturbation Φ_{INT}, results in additional integrated export of $93 mmol N m^{-3}$ ($7.4 gC m^{-2}$, Table 4) about 20% greater than that of Φ_{FLUX}. The maximum export flux occurs at the time of perturbation, i.e., the maximum instantaneous amplification factor is less than 1. As in the response to Φ_{FLUX}, the slow decay of P_2, which is exported to higher trophic levels, is the primary reason for the large integrated export.

d. Non-optimal perturbation: Proportional increase in P_1 and P_2

The optimal perturbation in only P_1 and P_2, Φ_{FLUX-P}, resulted in increased integrated export from the ecosystem relative to steady state (Table 4), and was primarily an increase in P_2. To investigate the dependence of perturbation evolution on initial conditions of our choosing, we consider an instantaneous bloom in both functional groups, $\Phi_{P_1 P_2}$, represented by an increase in both P_1 and P_2 proportional to the phytoplankton steady state values (Table 3). Many conditions that improve conditions for photosynthesis for one phytoplankton functional group will similarly benefit other groups and also increase their growth rates, potentially resulting in an initial increase in both size classes proportional to steady state values. This perturbation is not the result of any optimization problem, but is considered for comparison to the optimal perturbations.

i. Ecosystem Response. The linearized ecosystem response to $\Phi_{P_1P_2}$, shown in Figure 4d, is dominated by the predator-prey oscillations between Z_1 and P_1. Unlike the responses to Φ_{INT} and Φ_{FLUX}, the P_1 and Z_1 both drop below steady state levels. The P_2 anomaly decays by 71% to a relative minimum at 11.7 days. Weak oscillations follow, driven by the predator-prey cycle in P_1 and Z_1 (which influences Z_2 grazing rates). P_2 values do not drop below their steady state value at any time, and it takes about 56 days for the perturbed P_2 to decrease to 10% of the initial perturbation.

The N response to $\Phi_{P_1P_2}$ is much different than the responses to Φ_{FLUX}, Φ_{FLUX-P}, and Φ_{INT}, which by construction, optimized exports. Initially N concentrations decrease as biological uptake exceeds incoming N from upwelling, reaching a minimum at 4.1 days. This change in N is much smaller than the response to previous perturbations. Afterwards, N begins to increase rapidly while overall primary production decreases, reaching a maximum in excess of its steady state concentration at 14.0 days. Following this maximum, N decreases to below equilibrium, as primary production again increases above steady state.

ii. Export Response. All of the export components initially increase following $\Phi_{P_1P_2}$ (Figure 5d), with a maximum overall amplification factor of 4.5, although this perturbation reduces export flux for short time intervals. The integrated export in response to $\Phi_{P_1P_2}$ is $19 mmol N m^{-2}$ ($1.5 g C m^{-2}$), considerably less than the other perturbations discussed so far (Table 4). The maximum export flux in response to $\Phi_{P_1P_2}$ is $3.8 mmol N m^{-2} d^{-1}$, similar to the other perturbations, but unlike those previously discussed, the export flux oscillates around the steady state value

of $1.8 mmol N m^{-2} d^{-1}$, with a minimum export flux of $1.3 mmol N m^{-2} d^{-1}$. This different behavior occurs because the P_2 contribution to increased export flux relative to steady state is not large enough to offset the decrease in D and Z_1 contributions following the declines in P_1 blooms. These minima are responsible for the relatively low integrated export, which is 20% of the integrated export due to Φ_{INT}.

e. Non-optimal perturbation: Increase in P_1 alone

The perturbation $\Phi_{P_1P_2}$ is primarily an increase in P_1 (Table 3). Integrated export resulting from this perturbation is low compared to that from the optimal perturbations, which are primarily in P_2, and is not much higher than the integrated export from the ecosystem at steady state. This difference led us to investigate if increasing only P_1 results in feedbacks that actually reduce the integrated export below that which occurs when the ecosystem remains at steady state over an equal time period. Like $\Phi_{P_1P_2}$, this perturbation is not the result of an optimization, and will be referred to as Φ_{P_1}.

The ecosystem response to this perturbation, shown in Figure 4e, initially resembles that of $\Phi_{P_1P_2}$, but at 7.4 days the N anomaly becomes positive and remains slightly above zero as it decays. The concentration of N decreases when primary production is above steady state, and increases during periods when primary production is below steady state. Because, in general, export flux is highest during and following periods of high primary production, N concentration tends to decrease before periods of enhanced export flux and increase during periods of reduced export flux.

The maximum instantaneous export flux in response to Φ_{P_1} is $3.5 mmol N m^{-2} d^{-1}$ (Table 4), similar to the other perturbations, although the minimum export flux is the lowest at $0.9 mmol N m^{-2} d^{-1}$. There is one major export event in response to Φ_{P_1} (Figure 5e), which is followed by a rapid decline in export flux. The integrated export in response to Φ_{P_1} is nearly the same as integrated export from an ecosystem in steady state over an equivalent time period (Table 4). A perturbation that increases only P_1 has effectively no impact on the net export.

4. Discussion

While there are significant differences in detail between the ecosystem responses to the different optimal and non-optimal perturbations considered in the previous section, these responses share a number of common features. In particular, the small phytoplankton and zooplankton (P_1 and Z_1) are tightly coupled because of their similar specific growth rates. This tight coupling results in predator-prey cycles (in 5 dimensions, so these oscillations do not always orbit around the steady state as would be the case in a 2-dimensional system), and to indirect couplings between P_1 and P_2 mediated by the grazers. An increase in P_2 results in an increased mesozooplankton specific grazing rate such that the increased grazing pressure on Z_1 can lead to a decline in microzooplaknton biomass and a consequent increase in P_1. In contrast, an increase in P_1 will lead to an increase in Z_1 and therefore to a *decrease* in P_2 due to increased grazing pressure by Z_2.

For the optimal perturbations, the P_1 biomass remains near or above steady state, resulting in enhanced fluxes to higher trophic levels. For the perturbation maximising

integrated export flux, Φ_{INT}, Z_1 biomass remains below or near steady state: the resulting reduction in grazing pressure on P_2 allows for a more persistent bloom and enhanced net export flux. Note that those perturbations optimizing instantaneous export flux (Φ_{FLUX}, Φ_{FLUX-P}) are associated with strong oscillatory variability in the $P_1 - Z_1$ sector; the resulting substantial "blooms" are responsible for the large instantaneous export fluxes. In contrast, the perturbation that optimizes integrated export (Φ_{INT}) is much less variable. (Figure 5).

For both non-optimal perturbations, $\Phi_{P_1P_2}$ and Φ_{P_1}, the magnitude of the predator prey oscillations is larger than was the case for the optimal perturbations, and P_1 and D biomasses oscillate about steady state. The low P_2 biomass in these perturbations reduces grazing pressure of Z_2 on Z_1, allowing the microzooplankton to rapidly graze down the P_1 and terminate the bloom. The predator-prey cycles have a visible (but small) effect on N concentrations.

Clearly, the choice of zooplankton grazing function results in unexpected relationships between state variables, and the mathematical formulation of these functions is not well constrained by observations (Gentleman *et al.*, 2003). In the present model Z_1 are not allowed to graze on P_2; Denman *et al.* (2006) allow for this grazing pathway at a low preference. If this pathway were included in our model the relationships between the phytoplankton state variables could change. Furthermore, alternate formulations of the specific grazing rate could possibly eliminate some of the indirect relationships between planktonic classes not directly linked by a predator/prey relationship.

There are also similarities between the export responses to the optimal perturba-

tions: all result in integrated export significantly above steady state (Table 4) such that the flux to higher trophic levels is the greatest contributor and aggregation is insignificant. The majority of export components remain above steady state in response to all optimal perturbations: anomalies in both Z_2 grazing on P_2, and sinking D remain positive (Figure 5), and these fluxes are large enough to offset the decrease in Z_2 grazing when when Z_1 biomass ventures below steady state. The additional integrated export in response to Φ_{FLUX} and Φ_{FLUX-P} is 20% less than Φ_{INT} (Table 4), suggesting that as long as the perturbation is largely an increase in P_2, the other components do not significantly decrease the achievable integrated export.

For both non-optimal perturbations ($\Phi_{P_1P_2}$, Φ_{P_1}), sinking D and predation by Z_2 on Z_1 oscillate about steady state. Although increases in primarily P_1 result in export events with high instantaneous flux, the flux of P_2 to higher trophic levels is insufficient to offset these minima and keep net export above steady state.

The persistence of large phytoplankton has been found to be an important contributor to integrated export, both directly through sinking and grazing fluxes to Z_2, and indirectly through suppressing Z_1 biomass (through an increase in Z_2 specific grazing rate) allowing greater primary productivity by P_1. In nature, the P_2 decay time scales are likely to be much shorter due to dilution from advection and mixing. We note that our model setup is similar to that of GCMs, in that the horizontal resolution of these models is coarse relative to the physical exchanges being modelled. A consequence of the coarse resolution is that the importance of P_2 to export flux may be increased in the model relative to its importance in the natural system. Furthermore, the iron limitation parameter is held constant in this study, further in-

creasing the persitence of P_2 blooms relative to those observed in nature (where iron limitation is not static). When iron limitation is considered in contemporary global biogeochemical models, iron limitation parameters vary spatially but not temporally (e.g. Zahariev *et al.*, 2008), and it is possible that these models also overestimate primary production at some locations, and thus export.

It is generally believed that large phytoplankton are the primary contributor to export via flux to higher trophic levels and sinking particles (e.g. Michaels and Silver, 1988), even in conditions where primary production is dominated by small phytoplankton. In this model, small phytoplankton do not directly contribute to export flux (12), but P_1 do contribute to all components of export flux indirectly. A portion of P_1 that is grazed by the microzooplankton is not assimilated and becomes D, which sinks, forms aggregates, and is grazed on by Z_1. Some of the P_1 and D biomass that is assimilated by Z_1 will be exported to higher trophic levels as Z_2 graze on Z_1. Our analysis is consistent with the findings of Richardson and Jackson (2007), who suggest that the relative contributions of all phytoplankton to export, directly and indirectly, are proportional to their net primary production, and the importance of small phytoplankton to export flux may be underestimated in current models.

Export flux due to aggregation of microphytoplankton and detritus was found to make a negligible contribution to export flux in this study. Of course, this conclusion depends on the fidelity with which the process of aggregation is modelled. We note that although the aggregation coefficient w_A is small ($0.02 mmol N^{-1} m^3 d^{-1}$), increasing this parameter to $0.1 mmol N^{-1} m^3 d^{-1}$ (Ruiz *et al.*, 2002) has a negligible effect

on the ecosystem dynamics and optimal perturbations, and aggregation remains the smallest contributor to export flux (not shown).

In the analysis considered in this study, both the perturbation dynamics and perturbation export fluxes have been linearized. We tested the reasonableness of the assumption of locally linear dynamics by investigating the differences between the linear and nonlinear dynamics for perturbations of norm $0.5 mmol N m^{-3}$ (Healey, 2008). On the whole, the linearizations were qualitatively accurate approximations to the fully nonlinear dynamics, especially the linearization of export flux. Although there exists literature on nonlinear optimal perturbations (e.g. Mu *et al.*, 2003), the analysis of linear responses to perturbations ensures that results are independent of perturbation magnitude.

5. Conclusions

This study has considered the response of an idealized planktonic ecosystem model to perturbations in the initial conditions. In particular, an analysis of the linearized dynamics around a stable steady state of the system, that is similar to obervations of the natural system, allowed the diagnosis of those initial perturbations which resulted in maximum amplification of instantaneous export flux and those which resulted in maximum net export over the duration of the perturbation. The following primary results were obtained:

- Perturbations to planktonic ecosystems may display dramatic transient growth, as measured by export flux, and a consideration of dynamics linearised locally around a steady stable state allows the computation of those perturbations

which lead to the largest export response.

- There is no simple relationship between amplification, maximum instantaneous export flux, and integrated export flux. Some perturbations resulted in a high initial increase in export but did not have significant net export flux, others had large net flux but not strong amplification.

- This study reinforces the complexity of interactions between components even in a linearized model; important aspects of the ecosystem responses such as export flux were sensitive to the structure of the perturbations.

- The flux to higher trophic levels was the dominant export flux. This result could be partly an artifact of the ecosystem model, but it is consistent with new observational studies (Richardson and Jackson, 2007). The indirect contribution of small phytoplankton to export flux is comparable to the contribution of the large phytoplankton.

- This study reinforces the importance of Z_1 in modelled fluxes and trophic interactions due to its direct and indirect role in trophic transfers (see Results). In general, microzooplankton are poorly sampled and their role in observed ocean ecosystem is not well understood (relative to those of other components of the ecosystem). The results of this study provide further support for more detailed observation of this component of the ecosystem.

This analysis yields relationships between state variables that are not obvious. It would be useful to investigate how export dynamics would change were a different

ecosystem model used, particularly a model with different grazing formulations and trophic interactions. Results could elucidate key differences between models and give an indication of the generality of the conclusions obtained with the present model. Another natural extension of this study would be to perform a similar analysis to an ecosystem model that includes different carbon compounds, and a functional group of calcifying phytoplankton. Furthermore, this model is set in the open ocean, and the parameters are tuned for a HNLC area where the effects of nutrient limitation are assumed constant. Because the ecosystem was not N limited in steady state, the response of N to perturbations did not affect the dynamics of other state variables. This type of analysis could be used to study the transient dynamics of other open ocean regions or coastal ecosystem models, which may be limited by N, and possibly other nutrients, and are subject to different sources of perturbations.

The response of this ecosystem model to perturbations provides insight into how planktonic ecosystems may respond to natural variability, and how ecosystem models may respond to a changing environment when coupled with GCMs. Because these models are being used to predict future climate scenarios, it is important to study their internal dynamics and the effects of these dynamics on carbon fluxes in ocean models.

Acknowledgments. The authors would like to thank the Natural Sciences and Engineering Research Council of Canada (NSERC), Fisheries and Oceans Canada, and the University of Victoria for funding. They would also like to thank Ken Denman and Andrew Edwards for their feedback and thoughtful comments.

Appendix A: Model Description

The planktonic ecosystem model considers 2 functional groups of phytoplankton: nanophytoplankton(flagellates, P_1) and microphytoplankton (diatoms, P_2), 2 functional types of zooplankton; microzooplankton (Z_1) and mesozooplankton (Z_2, which is specified), and detritus (D). The single prognostic nutrient is nitrogen (N), which is also the model currency. The evolution of these 5 state variables is given by the following set of differential equations:

$$\frac{dP_1}{dt} = \nu P_1 - \gamma_1 \frac{P_1}{P_1 + p_D D} Z_1 \tag{2}$$

$$\frac{dP_2}{dt} = \nu P_2 - \gamma_2 Z_2 \frac{P_2}{P_2 + Z_1} - m_{pd} P_2 - w_A (P_2^2 + \frac{2P_2}{P_2 + D} P_2 D) \tag{3}$$

$$\frac{dZ_1}{dt} = g_a \gamma_1 Z_1 - \gamma_2 Z_2 \frac{Z_1}{P_2 + Z_1} - m_{za} Z_1 \tag{4}$$

$$\frac{dD}{dt} = m_{pd} P_2 + (1 - g_a)\gamma_1 Z_1 - \gamma_1 \frac{p_D D}{P_1 + p_D D} Z_1 - r_e D - w_D D - w_A (D^2 + \frac{2D}{P_2 + D} P_2 D) \tag{5}$$

$$\frac{dN}{dt} = -\nu(P_1 + P_2) + r_e D + m_{za} Z_1 + m_{ca} \gamma_2 Z_2 + \frac{v_{UW}}{d_{ML}} (N_0 - N) \tag{6}$$

The parameter values used in this study are given in Table 5. The phytoplankton

specific growth rate, ν, is given by Liebig's law of the minimum:

$$\nu = \nu_{max} min(\frac{N}{k_n + N}, L_{fe}) \tag{7}$$

where ν_{max} is the maximum growth rate in the absence of nutrient limitation and k_N is a nitrogen half-saturation constant. When growth is not limited by N, the parameter L_{fe} sets an upper limit on phytoplankton growth that represents limitation of a micronutrient such as iron. Because the model is set in summer conditions, it is assumed that light is not limiting at any time.

The microzooplankton, Z_1, graze on both P_1 and D with grazing rate

$$\gamma_1 = r_m \frac{(P_1 + p_D D)^2}{k_p^2 + (P_1 + p_D D)^2} \tag{8}$$

where p_D is the relative grazing preference of Z_1 on D over P_1 and k_p is the "half-saturation constant".

Mesozooplankton biomass is held fixed because Z_2 have relatively long life spans (order months to years) compared to Z_1, and biomass is unlikely to change in response to ecosystem changes on the time scales considered. However, the Z_2 grazing rate responds to changes in availability of P_2 and Z_1:

$$\gamma_2 = r_c \frac{(P_2 + Z_1)^2}{k_z^2 + (P_2 + Z_1)^2} \tag{9}$$

The mortality rate of P_2 to D, m_{pd}, is linear. Aggregation, i.e. the formation of marine snow (Alldredge and Silver, 1988), is represented by a quadratic term in

both P_2 and D. The assimilation efficiency of Z_1, i.e. the portion of grazed P that is converted to Z biomass, is denoted g_a; unassimilated matter, e.g. biomass lost to sloppy feeding, becomes D. Microzooplankton excrete N with specific rate m_{za}. The particulate nitrogen contained in detritus is converted to dissolved nitrogen at the specific remineralization rate r_e, and D sinks at rate w_D ($7.5md^{-1}$). A portion of the biomass grazed by Z_2 is immediately excreted to N at a rate of m_{ca}

Station P is located in the Alaskan Gyre, a region of weak upwelling (Pond and Pickard, 1983). Nitrogen is injected via upwelling and exchanged by mixing with water from below the mixed layer that has average nitrogen concentration N_0 at rate v_{UW}. Any dilution of other state variables by physical exchange is included in the linear growth and mortality rates. The physical parameters for the model are set to be broadly consistent with observations made at Station P in the summer, for those parameters for which these observations exist (Table 5).

Export from the ecosystem is given by the equation

$$Export = w_D D + \gamma_2 Z_2 + w_A (P_2 + D)^2 \tag{10}$$

The sinking D export flux depends linearly on D, however the flux to higher trophic levels and aggregation terms are nonlinear and so must be linearized about the steady state in order to perform the optimizations described in Appendix B. The export function for the ecosystem state is approximated using a Taylor series expansion:

$$Export(\mathbf{x}_0 + \Delta\mathbf{x}) \approx Export(\mathbf{x}_0) + \nabla Export(\mathbf{x}_0)^T \cdot \Delta\mathbf{x} \tag{11}$$

where $\mathbf{x}_0$ is the ecosystem steady state, $\Delta\mathbf{x}$ the perturbation to this state, and ∇ the gradient operator relative to the state variables. The linearized export is thus given by the equation

$$Export = Export(\mathbf{x}_0) + 0.22\Delta P_2 + 0.21\Delta Z_1 + 0.38\Delta D \tag{12}$$

where ΔP_2, ΔZ_1, and ΔD are the perturbations in large phytoplankton, small zooplankton, and detritus, respectively. The export rates are computed in units of $mmolNm^{-3}d^{-1}$ and a constant C:N ratio is assumed for P_2, Z_1, and D, so comparing nitrogen export rates is equivalent to comparing the carbon export rate. The Redfield C:N ratio for phytoplankton of 106:16 is used (Redfield *et al.*, 1963). Note that C:N may vary in time and for different forms of organic matter in the ocean, but on average it is well approximated by the Redfield ratio. Variations in the ratio are not modelled because the added complexity is not warranted or well-constrained (Sterner and Elser, 2002).

Appendix B: Optimal Perturbations

The system of equations (2) - (6) can be expressed as the autonomous system of first order ordinary differential equations

$$\frac{d\mathbf{x}}{dt} = \mathbf{f}(\mathbf{x}) \tag{13}$$

where $\mathbf{x}$=(P_1, P_2, Z_1, D, N) is the state vector. The dynamics of a small perturbation around a fixed point $\mathbf{x}_0$, $\Delta\mathbf{x} = \mathbf{x} - \mathbf{x}_0$, can be described by the linearized dynamics

$$\frac{d}{dt}\Delta\mathbf{x} = \mathbf{A}\Delta\mathbf{x}, \tag{14}$$

where $\mathbf{A}$ is the Jacobian of $\mathbf{f}(\mathbf{x})$ evaluated at $\mathbf{x}_0$, that is

$$A_{i,j} = \frac{\partial f_i(\mathbf{x})}{\partial x_j}|_{\mathbf{x}=\mathbf{x}_0} \tag{15}$$

The solution of (14) is

$$\Delta\mathbf{x}(t) = e^{At}\Delta\mathbf{x}_0 \tag{16}$$

Provided that $\mathbf{x}$ remains sufficiently close to $\mathbf{x}_0$, the linearized dynamics will be a good approximation to the evolution of the full nonlinear system (Perko, 2001).

a. Optimizing rates

If the equilibrium $\mathbf{x_0}$ is stable, then the real parts of the eigenvalues of $\mathbf{A}$ will all be negative and small perturbations to a stable steady state will eventually converge back to equilibrium. However, these perturbations may display transient growth over finite times if the matrix $\mathbf{A}$ is not normal (i.e. $\mathbf{A}\mathbf{A}^T \neq \mathbf{A}^T\mathbf{A}$, where $\mathbf{A}^T$ is the transpose of $\mathbf{A}$ (Farrell and Ioannou, 1996)). It is possible to solve for the perturbation that optimizes some measure of the size of the perturbation at a fixed time τ, subject to the constraint that the perturbation be of unit norm (under some metric) at time $t = 0$ (Tziperman and Ioannou, 2002). Let $\mathbf{R}$ be a matrix defining the perturbation norm to be optimized, so that the magnitude of the perturbation at time τ is given by

$$J(t) = \Delta \mathbf{x}_0^T (e^{A\tau})^T \mathbf{R} e^{A\tau} \Delta \mathbf{x}_0 \tag{17}$$

The optimal perturbation at time τ is defined as the initial perturbation $\Delta \mathbf{x}_0$ that maximizes $J(\tau)$ under the norm $\mathbf{R}$, subject to the constraint that the norm of this perturbation is unity under some nonsingular norm $\mathbf{S}$:

$$\Delta \mathbf{x}_0^T \mathbf{S} \Delta \mathbf{x}_0 = 1 \tag{18}$$

It follows from this constrained optimization problem that the optimal perturbations satisfy the generalized eigenvalue problem

$$(e^{A\tau})^T \mathbf{R} e^{A\tau} \Delta \mathbf{x}_0 = \lambda \mathbf{S} \Delta \mathbf{x}_0 \tag{19}$$

where λ is a Lagrange multiplier. That is, the eigenvector corresponding to the largest eigenvalue of the matrix

$$\mathbf{S}^{-1} (e^{A\tau})^T \mathbf{R} e^{A\tau} \tag{20}$$

will be the optimal perturbation at time τ under the norm $\mathbf{R}$. As the perturbation evolves, the amplification of the perturbation under $\mathbf{R}$ is defined as

$$Amp^2(t) = \frac{\Delta \mathbf{x}(t)^T \mathbf{R} \Delta \mathbf{x}(t)}{\Delta \mathbf{x}_0^T \mathbf{R} \Delta \mathbf{x}_0} \tag{21}$$

In this study, the norm $\mathbf{R}$ is the matrix containing the coefficients of the squared linear export flux (12). The instantaneous export flux is optimized subject to the

constraint that the initial biomass of the perturbation is unity. For the perturbation in all state variables, Φ_{FLUX}, $\mathbf{S}$ is the identity matrix, and for Φ_{FLUX-P}, entries involving state variables other than P_1 and P_2 are large to suppress contributions of the other state variables.

b. Optimizing integrated quantities

The above theory is used to optimize the magnitude of the instantaneous state of a system of equations under some measure. Because of the potential of planktonic ecosystems as carbon sinks, it is of interest to determine the perturbation that results in the maximum carbon export over some period of time, that is, the integrated export. Maximizing the instantaneous export flux is equivalent to maximizing its square (17). However, the perturbation that optimizes the integral of the squared export flux does not necessarily result in the highest integrated export (which might involve some cancellation between positive and negative anomalies in export flux), so a different approach is required. The previous optimization problem involves a bilinear operator in the state vector, whereas this problem optimizes a dot product, and is linear in the state vector .

It is possible to determine the unit perturbation $\Delta\mathbf{x}_0$ that maximizes the integral of the projection of the model state on some vector $\mathbf{y} = (y_1, y_2, ..., y_n)$, where n is the dimension of the model. The quantity to be optimized is

$$I = \int_0^\infty \mathbf{y} \cdot e^{At} \Delta\mathbf{x}_0 dt \approx \Delta t \sum_{\tau=0}^{\infty} \mathbf{y} \cdot e^{A\tau\Delta t} \Delta\mathbf{x}_0 \tag{22}$$

where Δt is the timestep. Thus, the quantity to be maximized is

$$\Delta t \sum_{\tau=0}^{\infty} \mathbf{y} \cdot e^{A\tau\Delta t} \Delta \mathbf{x}_0 + \lambda(\Delta \mathbf{x}_0^T \mathbf{S} \Delta \mathbf{x}_0 - 1) \tag{23}$$

where λ is a Lagrange multiplier, and $\mathbf{S}$ is the identity matrix, as in Section 3a. Let $M(\tau) = e^{A\tau\Delta t}$. Evaluating the dot product and setting the derivative with respect to $\Delta \mathbf{x}_0$ to 0 gives

$$\Delta \tilde{x}_{0j} = \sum_{\tau=1}^{\infty} \sum_{i=1}^{n} y_i M_{i,j}(\tau) \tag{24}$$

Setting

$$\mathbf{x}_0 = \frac{1}{|\Delta \tilde{\mathbf{x}}_0|} \Delta \tilde{\mathbf{x}}_0 \tag{25}$$

gives an initial perturbation of norm 1.

Note that optimizing the integrated export over the interval $[\tau - \Delta, \tau + \Delta]$ is equivalent to optimizing the instantaneous export flux at time τ as $\Delta \to 0$.

References

Alldredge, A. and M. Silver. 1988. Characteristics, dynamics and significance of marine snow. Progress in Oceanography, *20*, 41 – 82.

Archer, D., S. Emerson, T. Powell, and C. Wong. 1993. Numerical hindcasting of sea surface pCO_2 at weathership Station Papa. Progress in Oceanography, *32*, 319–351.

Boyd, P. and P. Harrison. 1999. Phytoplankton dynamics in the ne subarctic pacific. Deep-Sea Research Part II: Topical Studies in Oceanography, *46*, 2405 – 2432.

Boyd, P. W., C. S. Law, C. S. Wong, Y. Nojiri, A. Tsuda, M. Levasseur, S. Takeda, R. Rivkin, P. J. Harrison, R. Strzepek, J. Gower, R. M. McKay, E. Abraham, M. Arychuk, J. Barwell-Clarke, W. Crawford, D. Crawford, M. Hale, K. Harada, K. Johnson, H. Kiyosawa, I. Kudo, A. Marchetti, W. Miller, J. Needoba, J. Nishioka, H. Ogawa, J. Page, M. Robert, H. Saito, A. Sastri, N. Sherry, T. Soutar, N. Sutherland, Y. Taira, F. Whitney, S. K. E. Wong, and T. Yoshimura. 2004. The decline and fate of an iron-induced subarctic phytoplankton bloom. Nature, *428*, 549–553.

de Baar, H., P. Boyd, K. Coale, M. Landry, A. Tsuda, P. Assmy, D. Bakker, Y. Bozec, R. Barber, M. Brzezinski, K. Buesseler, M. Boye, P. Croot, F. Gervais, M. Gorbunov, P. Harrison, W. Hiscock, P. Laan, C. Lancelot, C. Law, M. Levasseur, A. Marchetti, F. Millero, J. Nishioka, Y. Nojiri, T. van Oijen, U. Riebesell, M. Rijkenberg, H. Saito, S. Takeda, K. Timmermans, M. Veldhuis, A. Waite, and C.-S.

Wong. 2005. Synthesis of iron fertilization experiments: From the iron age in the age of enlightenment. Journal of Geophysical Research Part C., *110*, 1–24.

Denman, K. and M. Pena. 2002. The response of two coupled one-dimensional mixed layer/planktonic ecosystem models to climate change in the NE subarctic Pacific Ocean. Deep-Sea Research Part II: Topical Studies in Oceanography, *49*, 5739–5757.

Denman, K. L., C. Voelker, M. A. Pena, and R. B. Rivkin. 2006. Modelling the ecosystem response to iron fertilization in the subarctic NE Pacific: The influence of grazing, and Si and N cycling on CO2 drawdown. Deep-Sea Research Part II: Topical Studies in Oceanography, *53*, 2327–2352.

Edwards, A. M. and J. Brindley. 1999. Zooplankton mortality and the dynamical behaviour of plankton population models. Bulletin of Mathematical Biology, *61*, 303–339.

Farrell, B. and P. Ioannou. 1996. Generalized stability theory. Part 1: Autonomous operators. Journal of the Atmospheric Sciences, *53*, 2025–2040.

Fasham, M. J. R. 1993. Modelling the marine biota. *In* Heimann, M., ed., The Global Carbon Cycle. Springer-Verlag, volume 73 Supp., pp. 457–504.

Gentleman, W., A. Leising, B. Frost, S. Strom, and J. Murray. 2003. Functional responses for zooplankton feeding on multiple resources: a review of assumptions and biological dynamics. Deep-Sea Research Part II: Topical Studies in Oceanography, *50*, 2847–2875.

Goldblatt, R. H., D. L. Mackas, and A. G. Lewis. 1999. Mesozooplankton community characteristics in the NE subarctic Pacific. Deep-Sea Research Part II: Topical Studies in Oceanography, *46*, 2619–2644.

Healey, K. 2008. Perturbation dynamics of a planktonic ecosystem. Master's thesis, University of Victoria.

Jo, C. O., J. Y. Lee, K. A. Park, Y. H. Kim, and K. R. Kim. 2007. Asian dust initiated early spring bloom in the northern East/Japan Sea. Geophysical Research Letters, *34*.

Martin, J., R. Gordon, and S. Fitzwater. 1991. The case for iron. Limnology & Oceanography, *36*, 1793 – 1802.

Martin, J., R. Gordon, S. Fitzwater, and W. Broenkow. 1989. VERTEX: Phytoplankton/iron studies in the Gulf of Alaska. Deep-Sea Research Part A., *36*, 649–680.

Michaels, A. F. and M. W. Silver. 1988. Primary production, sinking fluxes and the microbial food web. Deep-Sea Research Part A-Oceanographic Research Papers, *35*, 473–490.

Monahan, A. and K. Denman. 2004. Impacts of atmospheric variability on a coupled upper-ocean/ecosystem model of the subarctic Northeast Pacific. Global Biogeochemical Cycles, *18*. GB2010, doi:10.1029/2003GB002100.

Moore, J. K., S. C. Doney, and K. Lindsay. 2004. Upper ocean ecosystem dynam-

ics and iron cycling in a global three-dimensional model. Global Biogeochemical Cycles, *18*, 1–21.

Mu, M., W. S. Duan, and B. Wang. 2003. Conditional nonlinear optimal perturbation and its applications. Nonlinear Processes in Geophysics, *10*, 493–501.

Perko, L. 2001. Differential Equations and Dynamical Systems. Springer-Verlag, 538 pp.

Pitchford, J. W. and J. Brindley. 1999. Iron limitation, grazing pressure and oceanic high nutrient-low chlorophyll (HNLC) regions. Journal of Plankton Research, *21*, 525–547.

Pond, S. and G. L. Pickard. 1983. Introductory Dynamical Oceanography. Butterworth-Heinemann, 349 pp.

Redfield, A. C., B. H. Ketchum, and F. A. Richards. 1963. The influence of organisms on the composition of sea-water. *In* Hill, M., ed., The sea: Ideas and observations on progress in the study of the seas. John Wiley and Sons, New York, pp. 26–77.

Richardson, T. L. and G. A. Jackson. 2007. Small phytoplankton and carbon export from the surface ocean. Science, *315*, 838–840.

Ruiz, J., L. Prieto, and F. Ortegon. 2002. Diatom aggregate formation and fluxes: a modeling analysis under different size-resolution schemes and with empirically determined aggregation kernels. Deep-sea Research Part I-Oceanographic Research Papers, *49*, 495–515.

Saito, H., A. Tsuda, Y. Nojiri, J. Nishioka, S. Takeda, H. Kiyosawa, I. Kudo, Y. Noiri, T. Ono, Y. Taira, K. Suzuki, T. Yoshimura, and P. W. Boyd. 2006. Nutrient and phytoplankton dynamics during the stationary and declining phases of a phytoplankton bloom induced by iron-enrichment in the eastern subarctic pacific. Deep-Sea Research Part II: Topical Studies in Oceanography, *53*, 2168–2181.

Sarmiento, J. L. and N. Gruber. 2006. Ocean Biogeochemical Dynamics. Princeton University Press, 526 pp.

Schmittner, A., A. Oschlies, X. Giraud, M. Eby, and H. Simmons. 2005. A global model of the marine ecosystem for long-term simulations: Sensitivity to ocean mixing, buoyancy forcing, particle sinking, and dissolved organic matter cycling. Global Biogeochemical Cycles, *19*, 1–17.

Steele, J. 1974. The Structure of Marine Ecosystems. Harvard University Press, 128 pp.

Sterner, R. W. and J. J. Elser. 2002. Ecological Stoichiometry: The Biology of Elements from Molecules to the Biosphere. Princeton University Press, 584 pp.

Truscott, J. E. and J. Brindley. 1994. Ocean plankton populations as excitable media. Bulletin of Mathematical Biology, *56*, 981–998.

Tziperman, E. and P. J. Ioannou. 2002. Transient growth and optimal excitation of thermohaline variability. Journal of Physical Oceanography, *32*, 3427 – 3435.

Volk, T. and M. Hoffert. 1985. Ocean carbon pumps - Analysis of relative strengths and efficiencies in ocean-driven atmospheric CO2 changes. *In* Sundquist, E. and

W. Broecker, eds., The Carbon Cycle and Atmospheric CO_2: Natural variations Archean to Present, AGU, Washington, D.C., volume 32 of *Geophysical Monograph Series*. pp. 99–110.

Volterra, V. 1928. Variations and fluctuations of the number of individuals in animal species living together. ICES Journal of Marine Science, *3*, 3–51.

Whitney, F. and H. Freeland. 1999. Variability in upper-ocean water properties in the NE Pacific Ocean. Deep-Sea Research Part II: Topical Studies in Oceanography, *46*, 2351–2370.

Wong, C. S., D. A. Timothy, C. S. Law, Y. Nojiri, L. S. Xie, S. K. E. Wong, and J. S. Page. 2006. Carbon distribution and fluxes during the SERIES iron fertilization experiment with special reference to the fugacity of carbon dioxide (fCO(2)). Deep-Sea Research Part II: Topical Studies in Oceanography, *53*, 2053–2074.

Wong, C. S., F. A. Whitney, D. W. Crawford, K. Iseki, R. J. Matear, W. K. Johnson, and J. S. Page. 1999. Seasonal and interannual variability in particle fluxes of carbon, nitrogen and silicon from time series of sediment traps at Ocean Station P, 1982-1993: relationship to changes in subarctic primary productivity. Deep-Sea Research Part II: Topical Studies in Oceanography, *46*, 2735–2760.

Zahariev, K., J. Christian, and K. Denman. 2008. A global ocean carbon model with novel parameterizations of iron limitation, calcification and N2 fixation: preindustrial, historical, and fertilization simulations. Progress in Oceanography, *77*, 56–82.

Table 1. Definition of frequently used symbols. Each Φ represents a perturbation experiment.

Table 2. Ecosystem state variable values for the only stable steady state of the 4 steady state solutions possible.

Table 3. Unit perturbations ($mmolNm^{-3}$) to steady state. The perturbation Φ_{FLUX} is in all state variables, optimizes instantaneous export flux, and gives high transient amplification. The perturbation Φ_{FLUX-P} is only in phytoplankton state variables, optimizes instantaneous export flux, and results in significant amplification. The perturbation Φ_{INT} optimizes integrated export flux. The perturbations Φ_{P_2}, $\Phi_{P_1P_2}$, and Φ_{P_1} are considered for comparison to the optimal perturbations

Table 4. Properties of export responses to perturbations: minimum and maximum export flux, and integrated export over 150 days (1 hr timestep) in response to perturbations, for perturbation of magnitude $0.5mmolNm^{-3}$. The values in Column 4 are calculated using a Redfield ratio of 106:16 C:N. Export fluxes are obtained by multiplying export per unit volume by mixed layer depth (20m). Column 5 represents the P_2 decay time.

Table 5. Model parameter values. Many ecosystem parameters have been tuned to agree with observations and are not well constrained. MD04=Monahan and Denman (2004), DP02=Denman and Pena (2002), W99=Whitney and Freeland (1999), A93= Archer *et al.* (1993) , CV=C. Voelker, pers. com., P-Hist=Station P historical data, Institute of Ocean Sciences Archive

t	Time
P_1	Small phytoplankton ($\leq 20\mu m$)
P_2	Large phytoplankton ($> 20\mu m$)
Z_1	Microzooplankton
D	Detritus
N	Nitrogen
Z_2	Mesozooplankton
Φ_{FLUX}	Maximizes instantaneous export flux, amplification
Φ_{FLUX-P}	Maximizes instantaneous export flux, amp.; restricted to P_1 and P_2
Φ_{INT}	Maximizes integrated export
Φ_{P_2}	Increase in only P_2
$\Phi_{P_1P_2}$	Proportional increase in P_1 and P_2
Φ_{P_1}	Increase in only P_1

Table 1.

	steady state values ($mmolNm^{-3}$)			
P_1	P_2	Z_1	D	N
0.5265	0.1105	0.4073	0.0919	8.3153

Table 2.

	P_1	P_2	Z_1	D	N
Φ_{FLUX}	0.0785	0.8160	-0.5641	-0.0989	-0.0005
Φ_{FLUX-P}	0.6423	0.7665	0	0	0
Φ_{INT}	-0.0009	0.9977	-0.0296	0.0616	-0.0040
Φ_{P_2}	0	1.0000	0	0	0
$\Phi_{P_1P_2}$	0.9807	0.1955	0	0	0
Φ_{P_1}	1.0000	0	0	0	0

Table 3.

	export flux $mmolNm^{-2}d^{-1}$		int. export $(mmolNm^{-2})$	int. export relative to steady state (gCm^{-2})	day such that $\Delta P_2(t) = .1\Delta P_2(0)$
	min	max			
Φ_{FLUX}	2.0	4.4	350	+6.1	75
Φ_{FLUX-P}	1.9	4.4	350	+5.7	73
Φ_{INT}	1.9	4.2	370	+7.4	75
Φ_{P_2}	1.9	4.1	370	+7.4	75
$\Phi_{P_1P_2}$	1.3	3.8	300	+1.5	56
Φ_{P_1}	0.86	3.5	280	+0.02	NA
Steady State	1.8	1.8	280	0	NA

Table 4.

		Value	Unit	Source
ν_{max}	maximum phyto. growth rate	1.5	d^{-1}	DP02
p_d	grazing preference of Z_1 on D	0.5	-	DP02
Z_2	Z_2 biomass	0.2	$mmolNm^{-3}$	DP02
m_{pd}	P_2 to D mortality	0.1	d^{-1}	MD04
m_{za}	Z_1 to N	0.1	d^{-1}	MD04
r_e	D remineralization rate	0.1	d^{-1}	DP02
m_{ca}	Z_2 grazing to N	0.3	-	DP02
r_m	maximum Z_1 grazing rate	1.0	d^{-1}	DP02
k_p	Z_1 grazing half-saturation const.	0.75	$mmolNm^{-3}$	DP02
r_c	maximum Z_2 grazing rate	6.5	d^{-1}	MD04
k_z	Z_2 grazing half-saturation const.	2	$mmolNm^{-3}$	MD04
N_0	average N below mixed layer	26.8	$mmolNm^{-3}$	P-Hist
k_n	P growth half-saturation const.	0.1	$mmolNm^{-3}$	DP02
L_{fe}	iron limitation coefficient	0.05	-	tuned
d_{ML}	mixed layer depth	20	m	W99
v_{uw}	upwelling velocity	.1	md^{-1}	A93
w_D	D turnover rate due to sinking	0.3750	d^{-1}	MD04
g_a	Z_1 assimilation efficiency	0.7	-	DP02
w_A	aggregation coefficient	0.02	$mmolN^{-1}m^3d^{-1}$	CV

Table 5.

Figure 1. Model dynamics. State variables include nitrogen (N), small phytoplankton (P1), large phytoplankton (P2), small zooplankton (Z1), large zooplankton (Z2, prescribed), and detritus (D). Bold arrows denote export: detritus sinks (1), detritus and large phytoplankton form aggregates (2), and large phytoplankton and small zooplankton are consumed by large zooplankton (3). In steady state these losses are balanced by the input of N via upwelling.

Figure 2. Maximum amplification of export flux following perturbations in all state variables that optimize export flux at time τ. The perturbation that gives the maximum amplification is Φ_{FLUX} and corresponds to the perturbation that optimizes export flux at $\tau = 9.3$ days.

Figure 3. Ecosystem response to perturbations Φ_{FLUX} (a), Φ_{FLUX-P} (b), Φ_{INT} (c), $\Phi_{P_1P_2}$ (d), and Φ_{P_1} (e) for the first 150 days following the perturbation at $t = 0$. The dashed lines show the steady state values for each state variable. In each panel, dark blue is P_1, green is P_2, red is Z_1, and teal is D.

Figure 4. Nitrogen response to perturbations Φ_{FLUX} (a), Φ_{FLUX-P} (b), Φ_{INT} (c), $\Phi_{P_1P_2}$ (d), and Φ_{P_1} (e) for the first 150 days following the perturbation at $t = 0$. Dashed lines show value at steady state.

Figure 5. Components of export flux anomaly (i.e. export flux anomaly at steady state is 0) in response to perturbations Φ_{FLUX} (a), Φ_{FLUX-P} (b), Φ_{INT} (c), $\Phi_{P_1P_2}$ (d), and Φ_{P_1} (e) for 150 days following the perturbation at $t = 0$.. The solid black line is net export, the solid grey line is sinking detritus, the dashed grey line is aggregation, and the dashed black line is flux to higher trophic levels.

Figure 6. Amplification (dimensionless, (21)) in response Φ_{FLUX} (solid black), Φ_{FLUX-P} (dashed black), Φ_{INT} (solid grey), and $\Phi_{P_1P_2}$ (dashed grey). The time of the perturbations is $t = 0$. Note that Φ_{P_1} is not included as amplification is infinite in response.

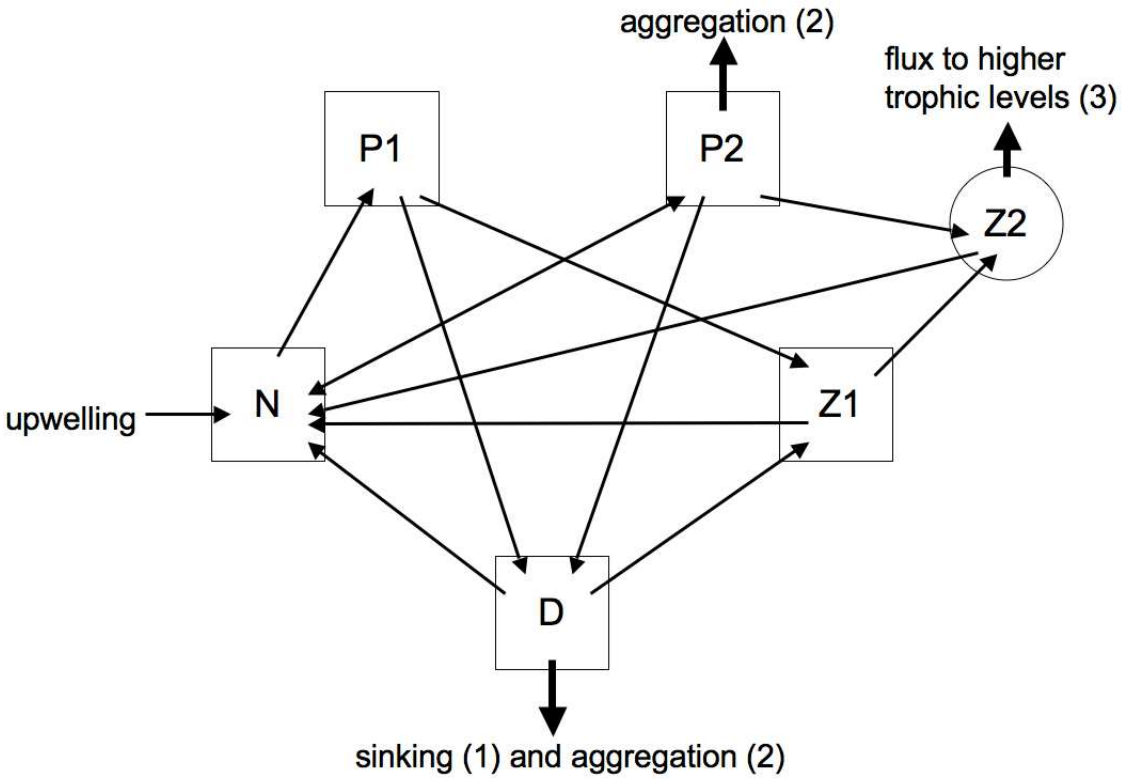
aggregation (2)
flux to higher
trophic levels (3)
P1
P2
Z2
upwelling
N
Z1
D
sinking (1) and aggregation (2)

Figure 1.

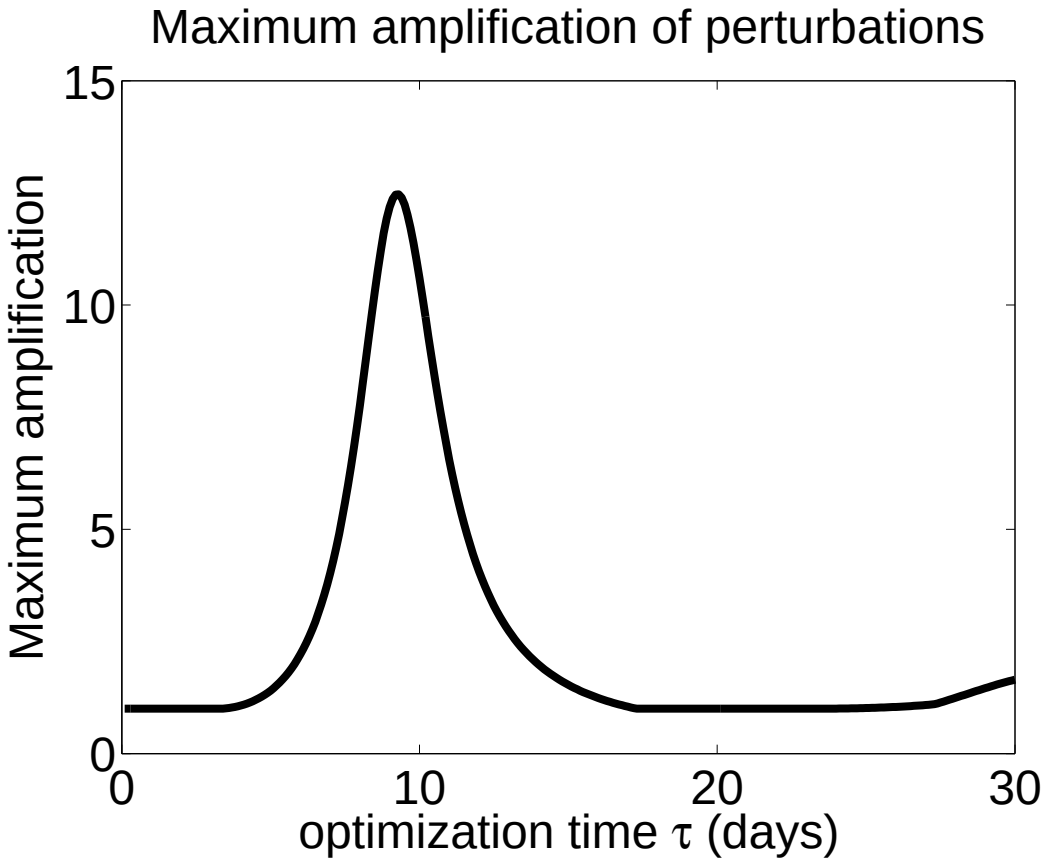
Maximum amplification of perturbations
Maximum amplification
15
10
5
0
0
10
20
30
optimization time τ (days)

Figure 2.

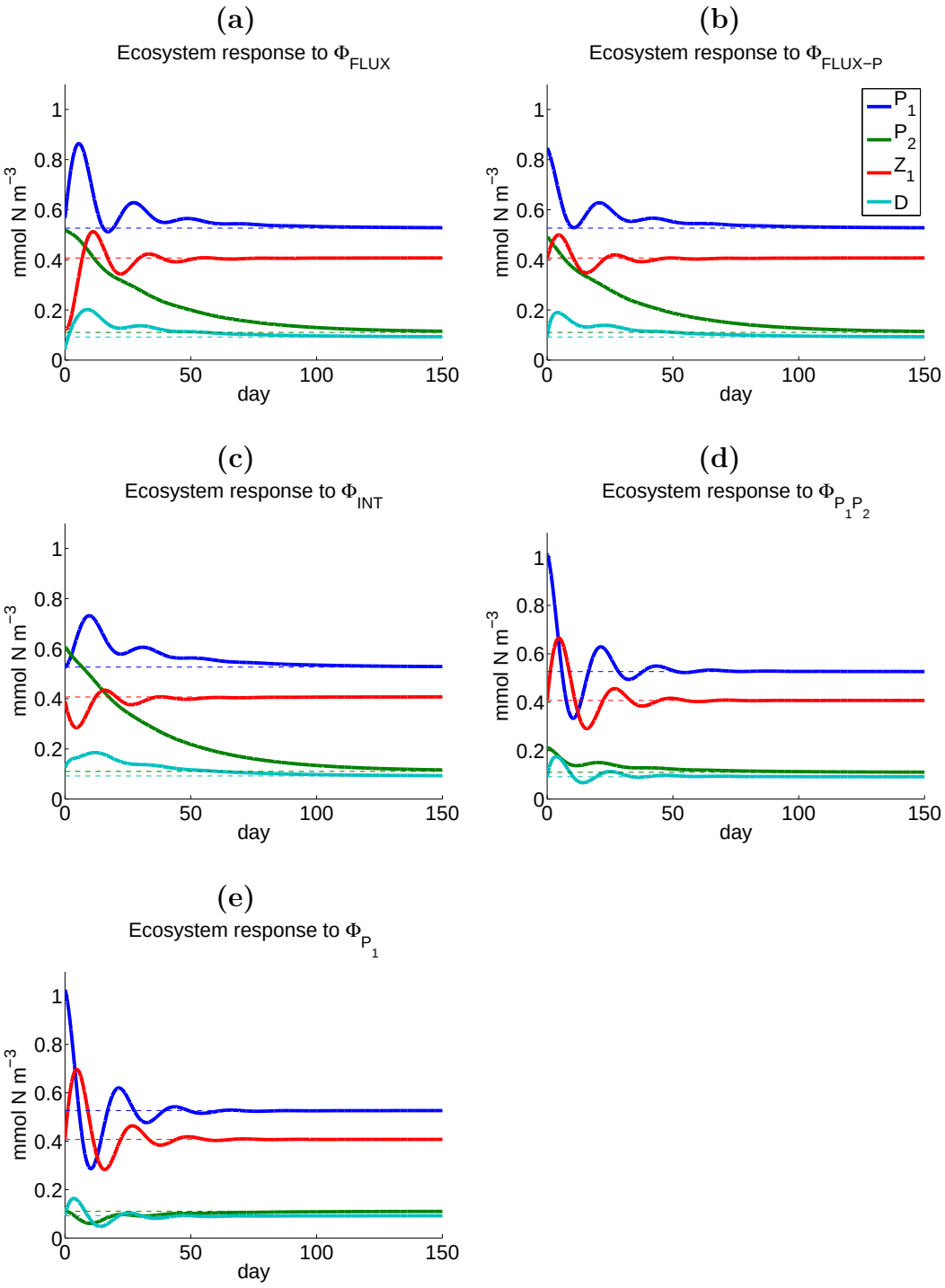
(a)
Ecosystem response to Φ_{FLUX}
(b)
Ecosystem response to Φ_{FLUX-P}
P_1
P_2
Z_1
D
(c)
Ecosystem response to Φ_{INT}
(d)
Ecosystem response to $\Phi_{P_1P_2}$
(e)
Ecosystem response to Φ_{P_1}
mmol N m^{-3}
day
0
0.2
0.4
0.6
0.8
1
0
50
100
150

Figure 3.

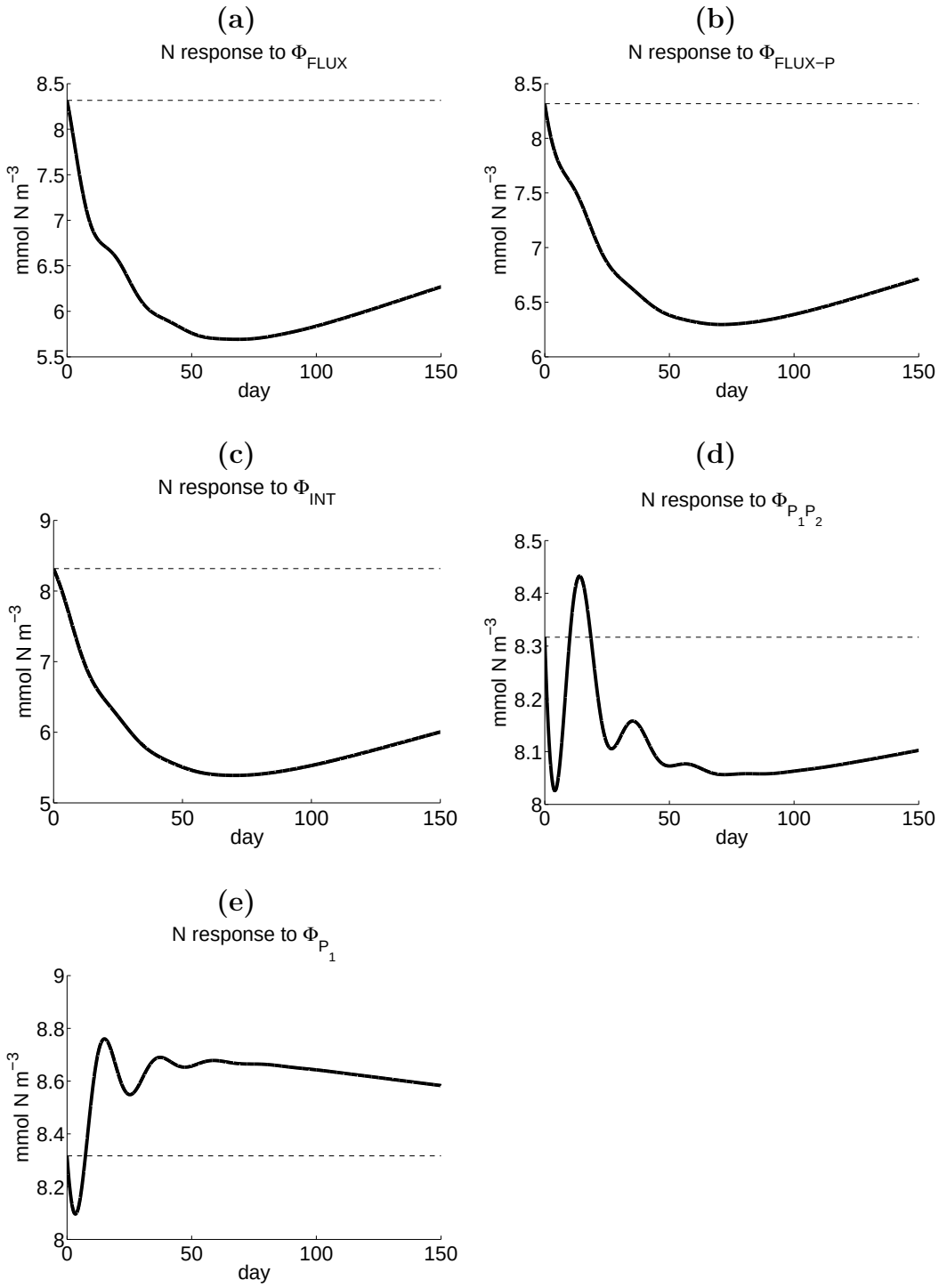
(a)
N response to Φ_{FLUX}
mmol N m^{-3}
day
(b)
N response to Φ_{FLUX-P}
mmol N m^{-3}
day
(c)
N response to Φ_{INT}
mmol N m^{-3}
day
(d)
N response to $\Phi_{P_1P_2}$
mmol N m^{-3}
day
(e)
N response to Φ_{P_1}
mmol N m^{-3}
day

Figure 4.

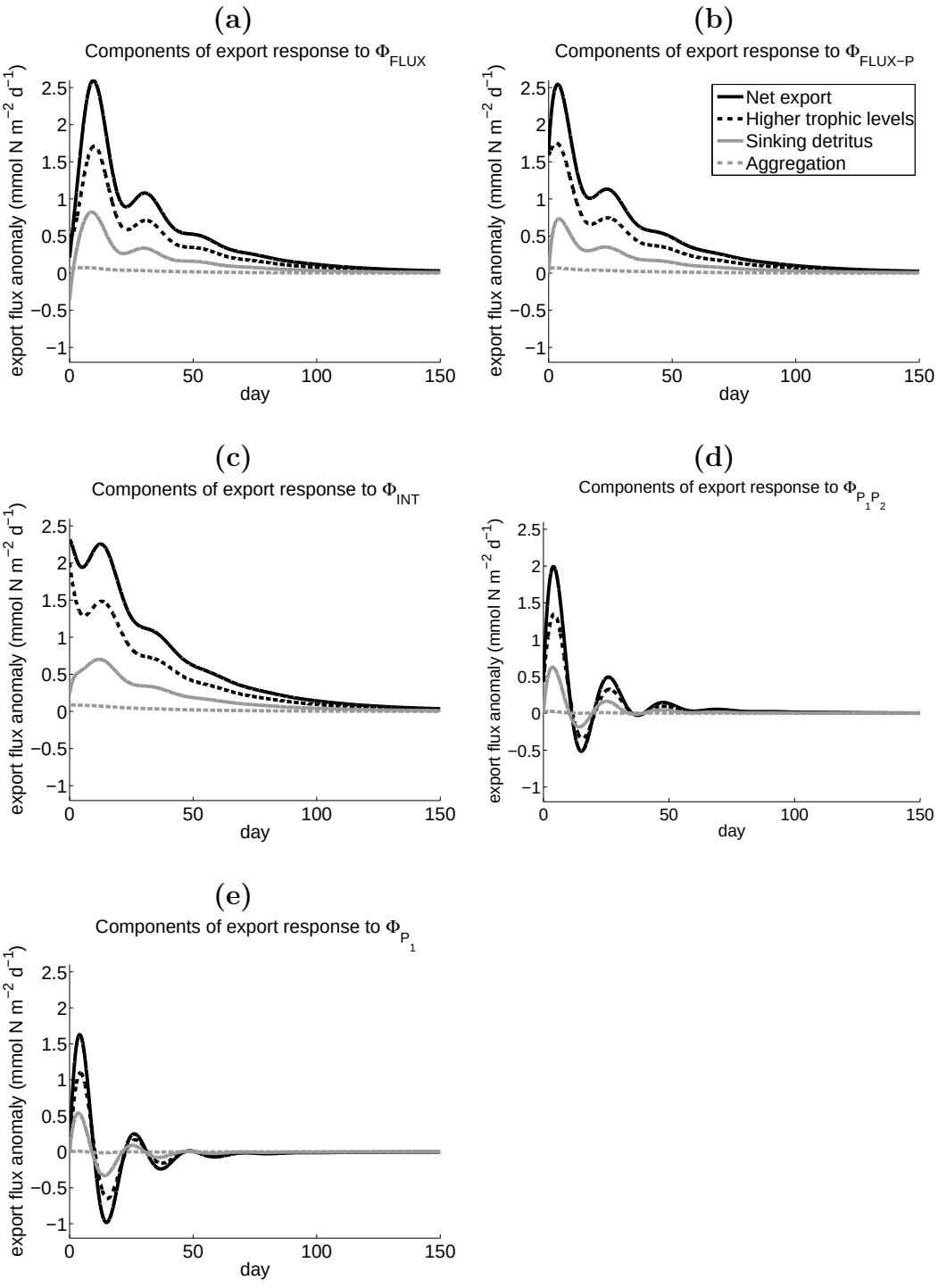
(a)
Components of export response to Φ_{FLUX}
(b)
Components of export response to Φ_{FLUX-P}
Net export
Higher trophic levels
Sinking detritus
Aggregation
(c)
Components of export response to Φ_{INT}
(d)
Components of export response to $\Phi_{P_1P_2}$
(e)
Components of export response to Φ_{P_1}
export flux anomaly (mmol N m^{-2} d^{-1})
day

Figure 5.

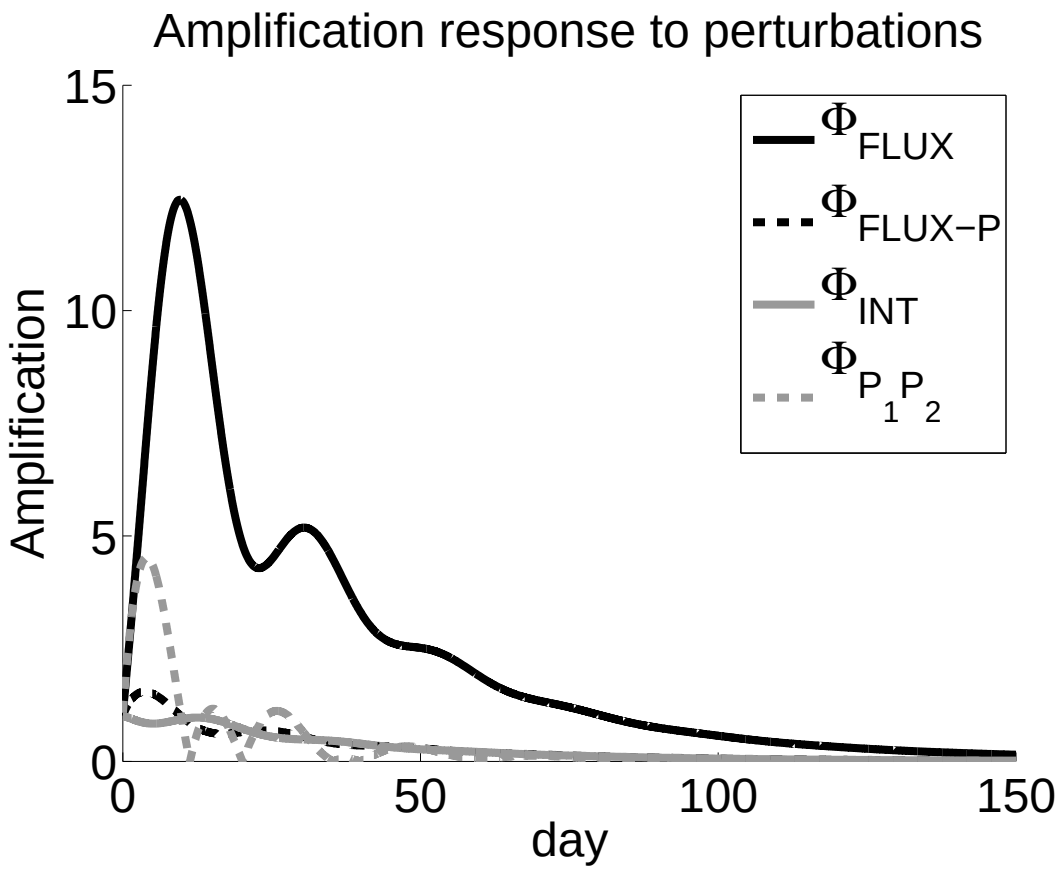
Amplification response to perturbations
15
10
5
0
Amplification
0
50
100
150
day
Φ_{FLUX}
Φ_{FLUX-P}
Φ_{INT}
$\Phi_{P_1P_2}$

Figure 6.